

Can a Carbon Nanotube Pierce through a Phospholipid Bilayer?

Sergey Pogodin[†] and Vladimir A. Baulin^{*,‡,†}

Departament d'Enginyeria Quimica, Universitat Rovira i Virgili 26 Av. dels Paisos Catalans, 43007 Tarragona, Spain, and ICREA, 23 Passeig Lluís Companys, 08010 Barcelona, Spain

E-mail: vladimir.baulin@urv.cat

Phone: +34 977 55 85 77. Fax: +34 977 55 96 21

Abstract

Great efficiency to penetrate into living cells is attributed to carbon nanotubes due to a number of direct and indirect observations of carbon nanotubes inside the cells. However, a direct evidence of physical translocation of nanotubes through phospholipid bilayers and the exact microscopic mechanism of their penetration into cells are still lacking. In order to test one of the inferred translocation mechanisms, namely the spontaneous piercing through the membrane induced only by thermal motion, we calculate the energy cost associated with the insertion of a carbon nanotube into a model phospholipid bilayer using the Single Chain Mean Field theory which is particularly suitable for the accurate measurements of equilibrium free energies. We find that the energy cost of the bilayer rupture is quite high compared to the energy of thermal motion. This conclusion may indirectly support other energy dependent translocation mechanisms such as, for example, endocytosis.

*To whom correspondence should be addressed

[†]Universitat Rovira i Virgili

[‡]ICREA

Keywords: phospholipid bilayer, carbon nanotubes, translocation mechanism, cell membrane

Phospholipid bilayers are designed by Nature to protect the interior of cells from the outside environment.^{1,2} Despite the weakness of hydrophobic interactions³ that drive the self-assembly of phospholipids into bilayers, cell membranes represent a serious protective barrier^{2,4} for external molecules, proteins, particles as well as artificial polymers and drugs. This barrier is quite efficient in protecting the interior of the cells and it is a challenging task to design nano-objects that can penetrate through the phospholipid bilayer without damaging its structure.⁵⁻⁸ If such nano-objects can be tailored, they can potentially be used for transmembrane delivery of active components into cells.⁹ However, the major difficulty lies in getting a direct microscopic information regarding the interaction of nano-objects with phospholipid layers at the molecular level in order to provide for physical mechanisms of nano-particle translocation across the membranes. In the absence of such microscopic information it is quite difficult to validate or distinguish between inferred translocation mechanisms that were proposed to explain the internalization by cells of several nano-objects such as, for example, cell penetrating peptides.¹⁰⁻¹³

Similarly, a consensus has not yet been reached regarding the translocation mechanism of carbon nanotubes through cell membranes. Single-walled carbon nanotubes (SWNTs) have been found inside the cells both in direct imaging experiments using electron microscope,^{14,15} spectroscopy¹⁶ and fluorescent microscopy studies.¹⁷⁻²⁶ Such experiments suggest that carbon nanotubes can efficiently penetrate into the cells, but very little can be said about the pathway and the entry mechanism regulating their internalization. Experimental efforts aimed to distinguish active and passive uptake include comparison of nanotubes internalization by living and dead cells,²⁷ change of the rate of active biological processes by temperature control,¹⁹ addition of selective chemical agents that inhibit active uptake,²⁰ and observing nanotubes on the cell membranes by Atomic Force Microscopy (AFM).²⁸

However, most of these experiments showing the translocation of carbon nanotubes, refer to biological membranes, which have complex structure, their properties depend on composition and many external parameters. Biological membranes may undergo several energy consuming pro-

cesses such as endocytosis²⁹ or phase transitions.² Thus, it is quite difficult to identify from these experiments a unique translocation mechanism and discard all other possibilities by studying a particular biological system. From this respect, the microscopic mechanism of nanotube translocation through the membrane remains an open question.

A study of a model system of a phospholipid bilayers without inclusions and comprising of one type of phospholipids may shed light on the plausibility of the spontaneous translocation of carbon nanotubes *via* rupture and diffusion of the phospholipid bilayer. If we assume that the driving force for the physical translocation of freely moving SWNTs through the homogeneous phospholipid bilayer is indeed thermal motion, then the energy barrier represented by the phospholipid bilayer should be comparable with the energy of thermal motion. Apparently, the energy barrier depends on the orientation of the SWNT with respect to the bilayer. The minimum energy would correspond to the positions inducing less perturbation to the phospholipid bilayer. Since in the perpendicular orientation to the bilayer plane the SWNT interacts with a minimal number of phospholipids, this orientation would have the minimal energy barrier. Other orientations would induce more perturbations to the bilayer and thus would require higher energies. Hence, an accurate estimation of the energy cost of the SWNTs perpendicular translocation through the phospholipid bilayer would allow to conclude about the possibility of such mechanism.

Calculation of equilibrium energies in computer simulations, that provide a microscopic information^{30–39} related to the structure and the dynamics of phospholipid bilayers is not straightforward, since the simulations usually deal with a limited number of molecules in the simulation box subject to fluctuations as well as due to the absence of a suitable reference state.^{40,41}

Alternative to computer simulations is the use of mean field type theories that do not include fluctuations and give direct access to the equilibrium free energies as a result of the minimization of the free energy functional. The Single Chain Mean Field (SCMF) theory^{42–45} is particularly suitable for such purposes and, in addition to the speed of calculation and high capability of parallelization, it can provide the microscopic details with the accuracy, competing with coarse-grained Monte Carlo (MC) and Molecular Dynamics (MD) simulations.

The numerical implementation of the SCMF theory was recently improved and the method was applied to model the equilibrium properties of the DMPC phospholipid bilayers in a fluid phase in Ref. 46. We use the 3-beads model of DMPC phospholipids of this work to model fluid phase of phospholipid bilayer and estimate the free energy of equilibrium insertion of the SWNT in a perpendicular direction to the bilayer plane using different diameters of carbon nanotubes and different parameters of interaction between nanotubes and the core of the bilayer. This gives the microscopic information about the possibility of spontaneous translocation of SWNTs through the phospholipid bilayer by thermal motion. Our model study has a broader interest than only study of biologically relevant translocation mechanisms. For example, AFM tip associated with a carbon nanotube can be used in order to quantify the force of the membrane rupture.^{47–50}

Free Energy of the Nanotube Insertion

The Single Chain Mean Field (SCMF) theory is relatively fast and stable tool for obtaining equilibrium properties and free energies of soft matter systems with different geometries and molecular structures.⁴⁶ A single molecule is described at a coarse grained level with explicit account of intramolecular interactions while the interactions between different molecules are described through mean molecular fields which are found self-consistently.

In the present work the phospholipid molecule is modeled within the 3-beads model with the interaction parameters obtained in Ref. 46. This model allows for spontaneous self-assembly of phospholipids in bilayers with realistic bulk bilayer properties such as the average interfacial area per lipid at equilibrium, the thickness of the bilayer and its hydrophobic core, and the compressibility constant. These thermodynamic properties rigidly fix the compression – extension energy curve,⁴⁶ the output of the SCMF calculations: the minimum of this curve gives the equilibrium area per lipid while its derivative is proportional to the compressibility constant. Thus, this curve gives us confidence in calculated values of the energy upon compression - extension of the bilayer.

The carbon nanotube is modeled as a rigid cylinder of a given diameter which is oriented per-

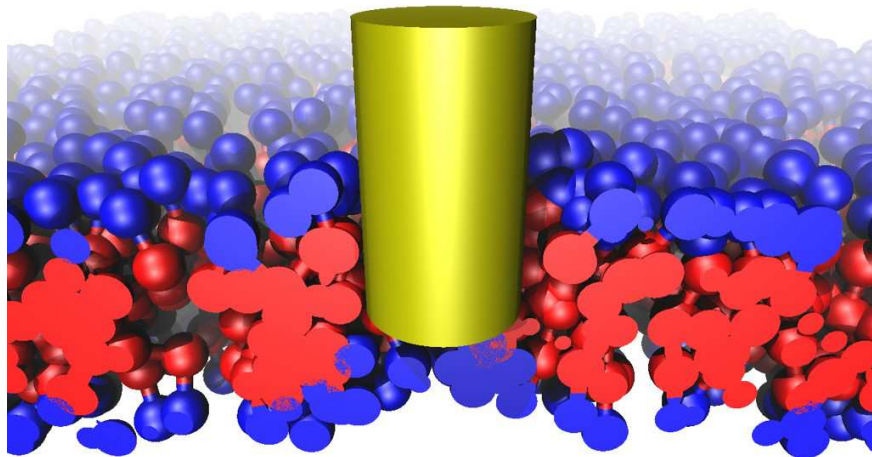


Figure 1: Mean field "snapshot" (set of most-probable conformations of the lipids) of the perpendicular SWNT insertion produced by the SCMF theory. Nanotube diameter 2.43 nm, nanotube position -0.63 nm, interaction parameter between the nanotube and the hydrophobic core $\varepsilon_T = -6.30$ kT.

pendicularly to the bilayer plane. More precisely, the carbon nanotube represents a cylindrical region in the simulation box, which is not accessible for phospholipids. We assume that the cylinder can interact with hydrophobic tails of phospholipids, because the driving force for the assembly of the phospholipid bilayer is the hydrophobic interactions and, thus, the interactions between the hydrophobic tails lead to the main contribution in the free energy.

The aim of this work is an accurate measurement of the energy cost of the presence of the SWNT at a fixed position from the bilayer plane. Since the SWNT can perturb the equilibrium structure of the bilayer, the free bilayer may ripple around, bend or displace in order to minimize the perturbation. In order to avoid such movements, the position of the bilayer in our model is restricted by non-interacting walls at the top and the bottom of the simulation box and the periodic boundary conditions are applied on the sides. Since the reference state for the free energy calculation is the energy of unperturbed phospholipid bilayer, we assume that the simulation box represents a small part of a much larger system, where the part of the bilayer outside the box is approximated by the

unperturbed bilayer which serves as a reference state. Thus, calculating the free energy of the small box, containing a part of the lipid bilayer, we can construct the free energy of the larger system. We write the total free energy of the system, F , as a sum of the free energy of the simulation box, F_{box} , and the free energy of the system outside the box, F_{out} , which, in turn, is expressed *via* the free energy density of the unperturbed bilayer given by the reference state, f_l^0 , and the entropy of pure solvent, $f_s = \frac{\phi_0}{v_s} \ln \frac{\phi_0}{v_s}$, where v_s is the volume of the solvent molecule and ϕ_0 is the bulk solvent volume fraction (see Ref. 46),

$$F = F_{box} + F_{out} = F_{box} + V_l^{out} f_l^0 + V_s^{out} f_s \quad (1)$$

The volume of the bilayer part lying outside of the simulation box, V_l^{out} , and the volume of pure solvent outside of the box, V_s^{out} , can be expressed *via* the volume of the unperturbed bilayer in the simulation box, V_l^0 , and the equilibrium numbers of lipids in the box with the cylinder, N_l , and without cylinder, N_l^0 . In addition, we take into account the conservation of the total volume of the system and the total number of lipid and solvent molecules. With this, f_l^0 is related to the free energy F_{box}^0 of the box containing the unperturbed bilayer as

$$f_l^0 = \frac{1}{V_l^0} (F_{box}^0 - (V_{box} - V_l^0) f_s) \quad (2)$$

while the free energy difference with respect to the reference state of unperturbed bilayer yields in the form

$$\Delta F = F_{box} - \frac{N_l}{N_l^0} (F_{box}^0 - V_{box} f_s) - (V_{box} - V_{cyl}^{in}) f_s \quad (3)$$

where V_{box} is the volume of the simulation box, and V_{cyl}^{in} is the part of the cylinder lying inside the box. We used 2D cylindrical geometry in order to discretize the space such that the symmetry axis coincide with the axis of the cylinder.

Results and Discussion

We have performed series of SCMF calculations for different positions of perpendicularly oriented SWNT with respect to the DMPC phospholipid bilayer plane for different diameters of the SWNT and interaction parameters between the SWNT and the core of the bilayer. The output of the calculations is the mean field concentration profiles of the heads and the tails in the bilayer, demonstrating the structural rearrangements of phospholipids induced by the SWNT at the molecular level and the precise measurements of the equilibrium free energy change for each position of the SWNT. In addition, the SCMF theory gives the probabilities of each phospholipid conformation in the corresponding mean fields. This information allows for visualization of the equilibrium molecular structure of the bilayer disturbed by the presence of the SWNT in form of mean field "snapshots" representing the most probable conformations of the molecules and their positions in the layer. One of such representative "snapshots" is shown in [figure][1][1].

Carbon nanotubes, by their chemical structure, can be considered as hydrophobic cylinders.⁵¹ Such objects in aqueous solutions tend to aggregate in bundles, which make difficult to observe individual SWNT in solution. In order to prevent such aggregation, the surface of the SWNT is often treated with acids or functionalized^{26,51} in such a way that they become slightly hydrophilic. That is why, the energy per contact of the hydrophobic bead with the nanotube, ϵ_T , in our calculations changes from 0, representing steric repulsion, to -6.3 kT, which corresponds to strong attraction (we assume the interaction distance 8.1 nm⁴⁶). Since SWNTs may have diameters ranging from 1 nm to 5 nm, we have chosen three diameters of the cylinder, 1.00 nm, 2.43 nm and 4.86 nm. The latter diameter is, probably, too big for SWNTs, but it may correspond to multi-walled nanotubes and we include it for completeness.

The free energy cost of the equilibrium insertion of the SWNT as a function of the distance between the SWNT tip and the middle plane of the unperturbed layer for different interaction parameters is shown in [figure][2][2]. Here the SWNT position -3.14 nm corresponds to the SWNT at the bilayer surface, while the position 3.14 nm corresponds to fully inserted SWNT. Insertion of slightly hydrophilic SWNT is not favorable and the free energy cost increases with the

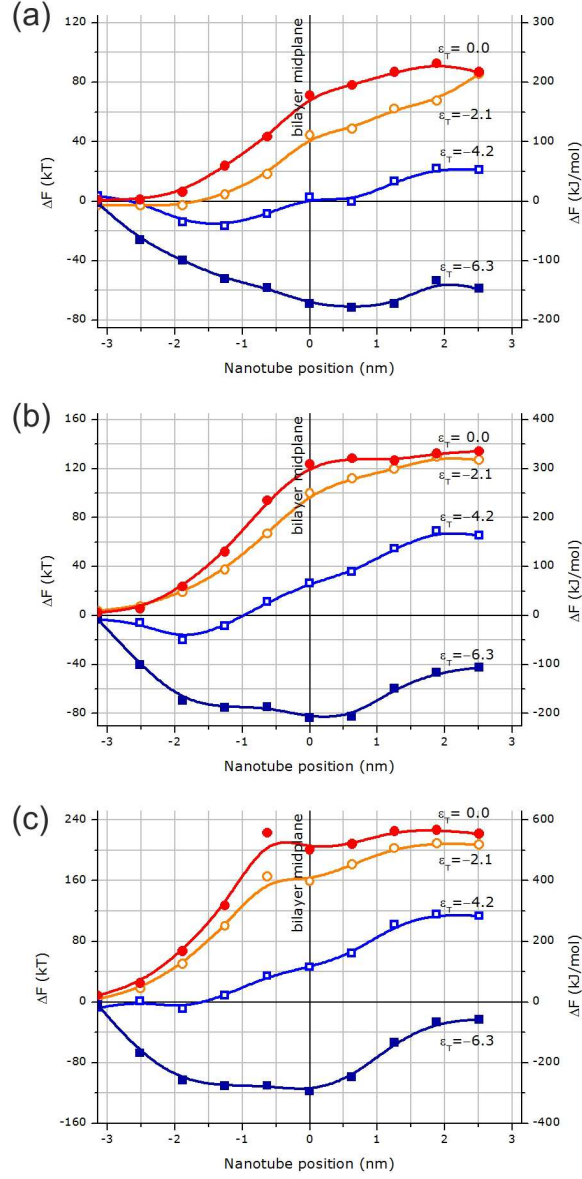


Figure 2: Free energy cost ΔF versus nanotube position of SWNTs with diameters 1 nm (a), 2.43 nm (b) and 4.86 nm (c) and different interaction parameters with the hydrophobic core of the phospholipid bilayer, ϵ_T .

insertion distance until the SWNT pierce completely the bilayer and the curve reaches the plateau, where the nanotube can slide along its length through the bilayer with no energy cost. In turn, the insertion of a hydrophobic SWNT is favorable and the corresponding insertion curve has a pronounced minimum which corresponds to the partial insertion of the nanotube into the bilayer when the hydrophobic bottom of the cylinder has maximum contacts with the phospholipid tails. It is noteworthy, that this minimum indicates that the perpendicular position of the hydrophobic nanotube would be less favorable than the parallel insertion into the core of the bilayer when the SWNT can have even larger number of contacts with the phospholipid tails. The corresponding free energy would be even more negative. The intermediate interaction parameters lead to mixed behavior, the energy gain at a partial insertion and the energy lost at a full insertion.

Inserted nanotube induces structural changes in the phospholipid bilayer. The SCMF theory allows to visualize the equilibrium structure of the bilayer at each position of the nanotube *via* equilibrium concentration profiles (see [figure][3][3]). One can see how the increasing hydrophobicity of the SWNT changes the character of the interaction with the bilayer and the structural changes around the SWNT. In case of steric repulsion ($\epsilon_T = 0.0$ kT) the cylinder compresses the bilayer and the tails tend to hide from the nanotube and the solvent, however hydrophobic SWNTs ($\epsilon_T = -2.1, -4.2, -6.3$ kT) attract hydrophobic core of the layer which tend to stick to the edges of the nanotube. The surface of the bilayer even lifts up in order to stick to the nanotube and increase the area of contact between the SWNT and the hydrophobic tails of the lipids. This is consistent with the corresponding decrease of the free energy upon insertion of the SWNT observed in [figure][2][2]. Full insertion of the nanotube leads to the pore formation. The energy of the pore formation as well as the structure of the pore strongly depends on the hydrophobicity of the nanotube ϵ_T . In the most hydrophilic case, the bilayer core is separated from the nanotube by the layer of heads, while in the most hydrophobic case, $\epsilon_T = -6.3$ kT, the tails touch the surface of the nanotube and one can observe the wetting of the nanotube with a pronounced rim around the nanotube. [figure][3][3] provides also information about the breakthrough distances. The hydrophilic nanotube creates a pore in the bilayer when it is inserted in the middle of the bilayer, in

Table 1: Free energy change due to full insertion of the SWNT, ΔF_{full} , the minimum free energy, ΔF_{min} , the insertion distance corresponding to the minimum of the free energy, d_{min} and the maximal force to be applied to pierce the bilayer.

| Diameter | 1.00 nm | | | | 2.43 nm | | | | 4.46 nm | | | |
|------------------------|---------|-------|-------|-------|---------|-------|-------|-------|---------|-------|-------|--------|
| ε_T (kT) | 0.0 | -2.1 | -4.2 | -6.3 | 0.0 | -2.1 | -4.2 | -6.3 | 0.0 | -2.1 | -4.2 | -6.3 |
| ΔF_{full} (kT) | 87.3 | 85.9 | 21.2 | -59.1 | 134.5 | 127.4 | 65.6 | -42.7 | 222.8 | 208.1 | 113.7 | -23.3 |
| ΔF_{min} (kT) | 0.8 | -3.0 | -16.7 | -72.1 | 2.3 | 3.8 | -20.3 | -83.8 | 8.6 | 3.5 | -9.0 | -118.6 |
| d_{min} (nm) | -3.14 | -2.51 | -1.25 | 0.63 | -3.14 | -3.14 | -1.88 | 0.00 | -3.14 | -3.14 | -1.88 | 0.00 |
| Max. force (pN) | 157 | 132 | 74 | 61 | 237 | 206 | 116 | 120 | 517 | 381 | 184 | 241 |

turn, hydrophobic nanotubes have to cross almost the full thickness of the bilayer before piercing it. This behavior is consistent with a similar observation in AFM experiments of AFM tip insertion in SOPC/cholesterol bilayers.⁵²

The numerical values of the free energy cost of translocation through the bilayer are summarized in [table][1][1]. The energy cost to cross the bilayer is quite high for all diameters and interaction parameters (hundreds kT). Hydrophilic nanotubes have a positive energy barrier, which may be difficult to overcome by thermal motion, while the attraction between hydrophobic nanotubes and phospholipid tails is high enough to entrap the nanotubes in the core of the bilayer. Nanotubes with intermediate hydrophobicity exhibit both effects, steric repulsion due to the pore formation and the enthalpic attraction to the core of the bilayer. Thus, the nanotubes with intermediate parameters will have to cross both barriers and the resulting energy cost is the sum of the two barriers. Furthermore, the perpendicular orientation of the nanotube has the lowest energy cost for penetration through the layer. This orientation is not necessary the equilibrium one. For example, the hydrophobic nanotube would preferentially orient itself parallel to the layer in the hydrophobic core, where the nanotube would have more contacts with the core. This orientation will have much lower energies, which are proportional to its length. Thus, we would expect that hydrophobic nanotubes with $\varepsilon_T = -4.2$ and -6.3 kT should stick in the hydrophobic core in a parallel orientation. In turn, hydrophilic nanotubes in a parallel orientation will have more steric contacts with both types of phospholipid beads. Thus, the positive barrier would be higher. The translocation through the bilayer also implies the diffusion of the nanotube in a correct orientation close to the bilayer. This would require additional time, thus effectively increasing the energy barrier.

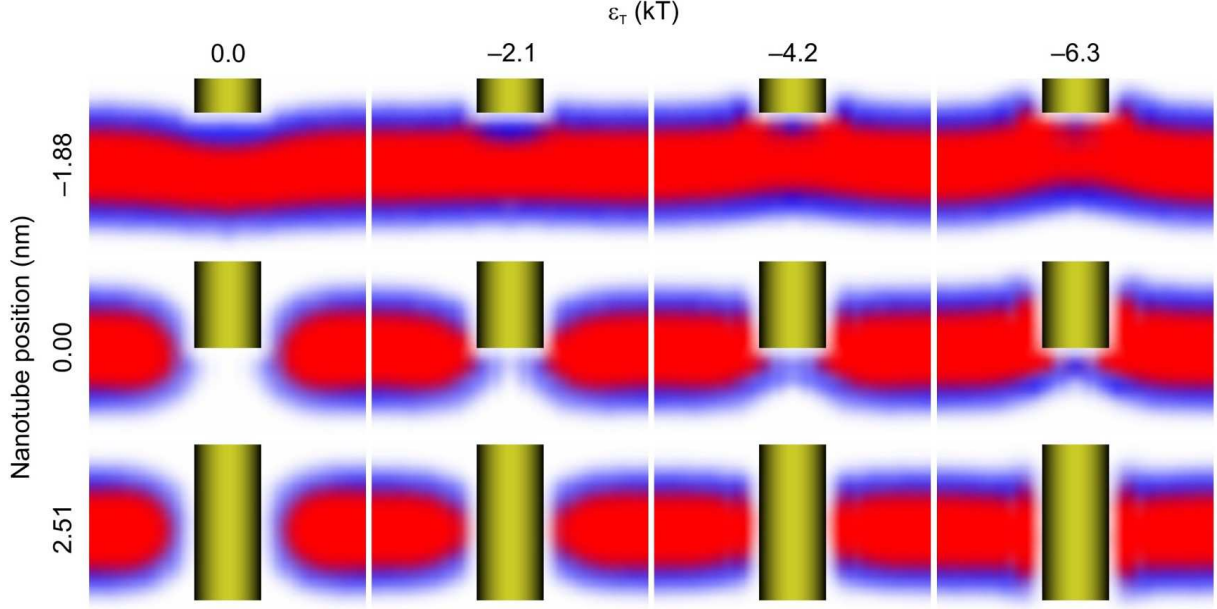


Figure 3: Morphology of the phospholipid bilayer structure induced by the equilibrium insertion of 2.43 nm SWNT for different interaction parameters between the nanotube and the hydrophobic core, ϵ_T .

High values of the energy barrier can be understood with the help of a simple estimation. If we consider that the cylinder with the radius $R_{cyl} = 1.2$ nm simply moves apart the lipids and creates a pore with the radius $R_{cyl} + R_{bead}$, where $R_{bead} = 0.4$ nm is the radius of the bead of in the phospholipid molecule, the pore formation energy is due to breaking contacts between phospholipids lying close to the edge of the pore. Taking into account that the perimeter of the pore is $2\pi(R_{cyl} + R_{bead}) \sim 10$ nm, the area per lipid is 60 \AA^2 , the energy per lipid due to tail-tail contacts in the 3-beads model is ~ -20 kT and assuming that lipids loose half of the contacts and the membrane is a double layer, we find that the number of lipids at the edge is ~ 26 , *i.e.* the energy cost for the formation of the pore is ~ 260 kT, which is comparable by the order of magnitude but higher than the calculated value of 192 kT. The discrepancy is due to contributions of the heads and the rearrangements of the lipids around the pore in order to minimize the energy cost, which does not have a sharp edge. Note, that this energy is comparable with the energy of breaking a chemical bond since typical values of bond energies are also hundreds kT.⁵³

The calculated equilibrium force of hundreds pN corresponds to the energy of hundreds kT, which is extremely high energy at the molecular level. However, the nanotube can pierce the phospholipid layer if the external force is applied. Carbon nanotubes can be fixed on AFM tip and they can be used as "nano-injectors" or nano-probes.⁴⁷ Such combination of AFM and carbon nanotube can be used for force measurements. The measurements on living cells⁴⁸ have shown that the force of penetration depends on the location over the cell membrane and, possibly, many other factors, especially if the cytoskeleton is involved in the response to the stimulus. The minimal force for piercing of cell membrane measured in these experiments is of order 100 pN, *i.e.* even higher than suggested by our calculations.

The strength of our method is the direct and accurate calculation of free energies at equilibrium, that allow for judgement about the possibility of spontaneous translocation through the bilayer. The forces obtained in non-equilibrium MD simulations of nanotube penetration with a constant speed⁵⁴ are several times higher than in our calculations and they depend on the speed of pulling, since the layer needs some time to accommodate its structure to the external perturbation. Hence, these calculations at low speed can represent an upper limit for the equilibrium free energy. In contrast, the SCMF method gives directly the equilibrium and average picture which does not show the positions of individual phospholipids but the average concentration profiles. That is why our equilibrium mean field "snapshots" and average concentration profiles look different from the simulation snapshots of non-equilibrium piercing.⁵⁴

The results with different diameters of nanotubes suggest that the thinner is a nanotube, the less is the energy barrier. Thus, we may conclude that larger objects such as multi-walled carbon nanotubes composed of several graphitic concentric layers⁵¹ and having diameters more than 4 nm will have even larger energy barrier, which require the application of an external force to pierce through the bilayer. Finally, an illustration of strong resistance of phospholipid bilayers against piercing is provided in the experiments with microtubules (rigid cylinders of 30 nm in diameter) growing inside the phospholipid vesicles.⁵⁵ Growing microtubule exert force on the inner wall of the vesicle at both ends, which leads to large deformation of the surface of the vesicle and the

buckling of the microtubule.

Conclusions

The SCMF theory is used for accurate measurements of the energy cost associated with the perpendicular insertion of carbon nanotubes of different diameters in the phospholipid bilayer. This method gives direct access to the equilibrium free energy and provides microscopic information about the structural rearrangements of the phospholipid bilayer around the inserted nanotubes. This information, though obtained for model DMPC phospholipid bilayers, may contribute to the discussion of the possible mechanisms of translocation of SWNTs into cells. In particular, it reflects on the inferred mechanism of spontaneous translocation of SWNTs through phospholipid bilayers by thermal motion.

Our results suggest that hydrophilic or non-interacting SWNTs would require the energy of order hundreds kT to cross the phospholipid bilayer in perpendicular orientation. Furthermore, perpendicular orientation is less disruptive for the bilayer and thus, other orientations would require even higher energies. In turn, more hydrophobic, interacting SWNTs are attracted by the hydrophobic cores, what hinders their translocation through the bilayers and renders difficult the separation of the nanotube from the bilayer simply by thermal motion. Thus, our results for model phospholipid bilayers may suggest that experimentally observed translocation of SWNTs into cells is probably due to other *energy dependent* translocation mechanisms such as, for example, endocytosis.

These results for homogeneous nanotubes may also indicate the ways to reduce the energy cost of translocation through the phospholipid bilayers. For example, inhomogeneous patterning of the nanotube surface can help in design of nano-objects which can freely pass through or preferentially associate with the phospholipid bilayers.

The predicted energy of the bilayer rupture due to the perpendicular insertion of a carbon nanotube can be directly verified by the force measurements of the insertion of the AFM tip func-

tionalized with a carbon nanotube.

Method: Single Chain Mean Field theory

The SCMF theory describes a single molecule surrounded by the mean fields.^{42–44,46} It takes explicitly into account the structure of an individual molecule at a coarse grained level similar to coarse grained MC or MD simulations. However, as distinct from simulations, the interactions of the molecule with the environment are described through the mean molecular fields. The mean fields determine the most probable conformations of the molecule through the probabilities of individual molecule. In turn, the mean fields are calculated as the average properties of individual conformations. This self-consistence closure defines the set of non-linear equations that can be solved numerically. The solution of such equations gives the equilibrium structures and the concentration profiles of all components in the system as well as the most probable conformations of individual molecules.

To model the phospholipid bilayer we use the 3-beads model of the DMPC phospholipid molecule described in Ref. 46. The phospholipid molecule is modeled as three spherical beads of diameter $d = 0.81$ nm, joined consequently by stiff bonds of 1.0 nm in length: two hydrophobic, T-beads, representing the tails, and one hydrophilic, H-bead, representing the phospholipid head. The angle between the bonds is free to bend as long as the terminal beads do not intersect each other. The solvent molecule is modeled as a S-bead of the same diameter as the phospholipid beads. The interactions between the beads in this model are given only by two square well potentials with interaction range $r_{int} = 1.215$ nm and depths $\epsilon_{TT} = -2.10$ kT for T-T contacts and $\epsilon_{HS} = -0.15$ kT for H-S contacts. Additional energy is assigned to the T-beads residing at a distance shorter than 8.10 nm from the surface of the cylinder, ϵ_T (see [table][1][1]). The simulation box $10.00 \times 10.00 \times 6.27$ nm ($12.00 \times 12.00 \times 6.27$ nm for the case of the largest nanotube’s diameter) is discretized into a grid according to 2D cylindrical geometry with the symmetry axis placed in the center of the box and oriented along the z -axis. The grid cells are about 0.5 nm in the radial

and 0.3 nm in the vertical directions (comparable with the diameters of the beads in the 3-beads model, 0.81 nm) and the sampling of the molecule conformational space is 400 000 conformations. A series of test calculations have shown that these parameters give enough precision for the energy calculations.

We use the generalized equations of the SCMF method provided in Ref. 46 which describes the self-assembly of a mixture of an arbitrary number of types of molecules of an arbitrary structure. First step of the SCMF method is the generation of the representative sampling $\{\Gamma\}$ of conformations of a single molecule, where the conformations differ in position and orientation of the molecule in the space and in the angle between the bonds of the molecule. If the sampling was generated with a bias, it is corrected with a known weight of each conformation $w(\Gamma)$. The probability of a given conformation Γ of the molecule, placed in the simulation box, containing N lipids is given by⁴⁶

$$\rho(\Gamma) = \frac{1}{Zw(\Gamma)} \exp \left(-H^{intra}(\Gamma) - (N-1) \sum_i \varepsilon_i^T(\Gamma) c_i^T - \sum_i \varepsilon_i^S(\Gamma) \frac{\phi_i^S}{v_s} + \sum_i V_i \lambda_i \phi_i(\Gamma) \right) \quad (4)$$

where Z is the normalization constant, $H^{intra}(\Gamma)$ is the internal energy of the conformation Γ , where we include, as well, its interaction with the nanotube. The simulation box is discretized into a grid cells i of the volume V_i . The interactions of the beads with the fields (c_i^T and c_i^H are the equilibrium concentrations of the beads of each type,) are described through interaction fields of a given conformation, $\varepsilon_i^T(\Gamma)$ and $\varepsilon_i^S(\Gamma)$. The Lagrange multiplier λ_i is related to the total volume fraction of the cell i occupied by the solvent, ϕ_i^S via $v_s \lambda_i = \ln \phi_i^S + N \varepsilon_i^H c_i^H$, where v_s is the volume of the solvent molecule and $\varepsilon_i^H = \frac{4}{3} \pi (r_{int}^3 - d^3) \varepsilon_{HS}$. The condition of local incompressibility relate ϕ_i^S with the volume fraction of the lipids ϕ_i via $\phi_i^S + N \phi_i = \phi_0$, where ϕ_0 is the maximal volume fraction occupied by the solvent and all the molecules (equal to 0.675 in this model).⁴⁶

Once the probabilities of the conformations $\rho(\Gamma)$ are known, the molecular mean fields, namely the volume fractions of the molecules and concentrations of the beads of all types, are calculated

as averages over all conformations,

$$\phi_i = \sum_{\{\Gamma\}} \phi_i(\Gamma) \rho(\Gamma) \quad (5)$$

$$c_i^{T(H)} = \sum_{\{\Gamma\}} c_i^{T(H)}(\Gamma) \rho(\Gamma) \quad (6)$$

These equations, ??, ??, ??, define the closed set of nonlinear equations for the probabilities of conformations and the mean fields. Solution of these equations gives the equilibrium properties of the system and the equilibrium free energy of the simulation box, which is written⁴⁶ in units kT as

$$\begin{aligned} F_{box} = & N \langle \ln N \rho(\Gamma) w(\Gamma) \kappa \rangle + \sum_i V_i \frac{\phi_i^S}{v_s} \ln \frac{\phi_i^S}{v_s} + N \langle H^{intra}(\Gamma) \rangle \\ & + \frac{1}{2} N(N-1) \sum_i \langle \epsilon_i^T(\Gamma) \rangle c_i^T + N \sum_i \langle \epsilon_i^S(\Gamma) \rangle \frac{\phi_i^S}{v_s} \end{aligned} \quad (7)$$

where κ is the number of conformations in the sampling $\{\Gamma\}$ and all the averages, denoted by angular brackets are taken as averages over the sampling with probabilities $\rho(\Gamma)$ in analogy to ?? and ??.

The calculation time of one point in the energy curve and full set of microscopic data of the bilayer configuration takes less than 1 day on a single 32-core machine. This time can be drastically decreased by taking advantage of high capability of parallelization of the SCMF method, which allows to use more computers and processors.

Acknowledgement

The authors wish to thank Prof. Nigel Slater from Cambridge University for useful discussions, suggestions, comments and collaboration within UK Royal Society International Joint Project with Cambridge University. We acknowledge the financial help from Spanish Ministry of education MICINN *via* the project CTQ2008-06469/PPQ.

Supporting Information Available

Structural changes in the phospholipid bilayer induced by the equilibrium insertion of a carbon nanotube for different distances of a nanotube from the bilayer midplane.

This material is available free of charge via the Internet at <http://pubs.acs.org/>.

References

1. Alberts, B. *Molecular Biology of the Cell*, 5th ed.; Garland Science: New York, 2008.
2. Yeagle, P. L. *The Structure of Biological Membranes*, 2nd ed.; CRC Press, 2005.
3. Tanford, C. The Hydrophobic Effect and the Organization of Living Matter. *Science* **1978**, *200*, 1012–1018.
4. Cooper, G. M.; Hausman, R. E. *The Cell: a Molecular Approach*, 5th ed.; Sinauer Associates Inc.: Sunderland, 2009.
5. Tew, G. N.; Liu, D.; Chen, B.; Doerksen, R. J.; Kaplan, J.; Carroll, P. J.; Klein, M. L.; De-Grado, W. F. De Novo Design of Biomimetic Antimicrobial Polymers. *Proc. of Nat. Acad. Sci.* **2002**, *99*, 5110–5114.
6. Stewart, K. M.; Horton, K. L.; Kelley, S. O. Cell-Penetrating Peptides As Delivery Vehicles for Biology and Medicine. *Org. Biomol. Chem.* **2008**, *6*, 2242–2255.
7. Moghimi, S. M.; Hunter, A. C.; Murray, J. C. Nanomedicine: Current Status and Future Prospects. *FASEB J.* **2005**, *19*, 311–330.
8. Kamada, H.; Okamoto, T.; Kawamura, M.; Shibata, H.; Abe, Y.; Ohkawa, A.; Nomura, T.; Sato, M.; Mukai, Y.; Sugita, T. et al. Creation of Novel Cell-Penetrating Peptides for Intracellular Drug Delivery Using Systematic Phage Display Technology Originated from Tat Transduction Domain. *Biol. Pharm. Bull.* **2007**, *30*, 218–223.

9. Pack, D. W.; Hoffman, A. S.; Pun, S.; Stayton, P. S. Design and Development of Polymers for Gene Delivery. *Nature* **2005**, *4*, 581–593.
10. Jenssen, H.; Hamill, P.; Hancock, R. E. W. Peptide Antimicrobial Agents. *Clinical Microbiol. Rev.* **2006**, *19*, 491–511.
11. Brogden, K. A. Antimicrobial Peptides: Pore Formers or Metabolic Inhibitors in Bacteria? *Nature* **2005**, *3*, 238–250.
12. Hancock, R. E. W.; Sahl, H.-G. Antimicrobial and Host-Defense Peptides as New Anti-Infective Therapeutic Strategies. *Nature Biotechnology* **2006**, *24*, 1551–1557.
13. Plank, C.; Zauner, W.; Wagner, E. Application of Membrane-Active Peptides for Drug and Gene Delivery across Cellular Membranes. *Advanced Drug Delivery Reviews* **1998**, *34*, 21–35.
14. Porter, A. E.; Gass, M.; Muller, K.; Skepper, J. N.; Midgley, P. A.; Welland, M. Direct Imaging of Single-Walled Carbon Nanotubes in Cells. *Nature Nanotechnology* **2007**, *2*, 713–717.
15. Porter, A. E.; Gass, M.; Bendall, J. S.; Muller, K.; Goode, A.; Skepper, J. N.; Midgley, P. A.; Welland, M. Uptake of Noncytotoxic Acid-Treated Single-Walled Carbon Nanotubes into the Cytoplasm of Human Macrophage Cells. *ACS Nano* **2009**, *3*, 1485–1492.
16. Khodakovskaya, M.; Dervishi, E.; Mahmood, M.; Xu, Y.; Li, Z.; Watanabe, F.; Biris, A. S. Carbon Nanotubes are Able to Penetrate Plant Seed Coat and Dramatically Affect Seed Germination and Plant Growth. *AcsNano* **2009**, *3*, 3221–3227.
17. Cherukuri, P.; Bachilo, S. M.; Litovsky, S. H.; Weisman, R. B. Near-Infrared Fluorescence Microscopy of Single-Walled Carbon Nanotubes in Phagocytic Cells. *J. Am. Chem. Soc.* **2004**, *126*, 15638–15639.

18. Kam, N. W. S.; Jessop, T. C.; Wender, P. A.; Dai, H. Nanotube Molecular Transporters: Internalization of Carbon Nanotube-Protein Conjugates into Mammalian Cells. *J. Am. Chem. Soc.* **2004**, *126*, 6850–6851.
19. Kam, N. W. S.; Dai, H. Carbon Nanotubes As Intracellular Protein Transporters: Generality and Biological Functionality. *J. Am. Chem. Soc.* **2005**, *127*, 6021–6026.
20. Kam, N. W. S.; Liu, Z.; Dai, H. Carbon Nanotubes As Intracellular Transporters for Proteins and DNA: An Investigation of the Uptake Mechanism and Pathway. *Angew. Chem. Int. Ed.* **2006**, *45*, 577–581.
21. Kam, N. W. S.; Dai, H. Single Walled Carbon Nanotubes for Transport and Delivery of Biological Cargos. *Phys. Stat. Sol. (B)* **2006**, *243*, 3561–3566.
22. Pantarotto, D.; Briand, J.-P.; Prato, M.; Bianco, A. Translocation of Bioactive Peptides across Cell Membranes by Carbon Nanotubes. *Chem. Commun.* **2004**, *1*, 16–17.
23. Pantarotto, D.; Singh, R.; McCarthy, D.; Erhardt, M.; Briand, J.-P.; Prato, M.; Kostarelos, K.; Bianco, A. Functionalized Carbon Nanotubes for Plasmid DNA Gene Delivery. *Angew. Chem. Int. Ed.* **2004**, *43*, 5242–5246.
24. Liu, Q.; Chen, B.; Wang, Q.; Shi, X.; Xiao, Z.; Lin, J.; Fang, X. Carbon Nanotubes as Molecular Transporters for Walled Plant Cells. *Nano Letters* **2009**, *9*, 1007–1010.
25. Lu, Q.; Moore, J. M.; Huang, G.; Mount, A. S.; Rao, A. M.; Larcom, L. L.; Ke, P. C. RNA Polymer Translocation with Single-Walled Carbon Nanotubes. *Nano Letters* **2004**, *4*, 2473–2477.
26. Raffa, V.; Ciofani, G.; Nitodas, S.; Karachalios, T.; D’Alessandro, D.; Masini, M.; Cuschieri, A. Can the Properties of Carbon Nanotubes Influence Their Internalization by Living Cells? *Carbon* **2008**, *46*, 1600–1610.

27. Kam, N. W. S.; O'Connell, M.; Wisdom, J. A.; Dai, H. Carbon Nanotubes As Multifunctional Biological Transporters and Near-Infrared Agents for Selective Cancer Cell Destruction. *Proc. of Nat. Acad. Sci.* **2005**, *102*, 11600–11605.
28. Lamprecht, C.; Liashkovich, I.; Neves, V.; Danzberger, J.; Heister, E.; Rangl, M.; Coley, H. M.; McFadden, J.; Flahaut, E.; Gruber, H. J. et al. AFM Imaging of Functionalized Carbon Nanotubes on Biological Membranes. *Nanotechnology* **2009**, *20*, 434001.
29. Miaczynska, M.; Stenmark, H. Mechanisms and Functions of Endocytosis. *J. Cell Biol.* **2008**, *180*, 7–11.
30. Goetz, R.; Lipowsky, R. Computer Simulations of Bilayer Membranes: Self-Assembly and Interfacial Tension. *J. Chem. Phys.* **1998**, *108*, 7397–7409.
31. Tieleman, D.; Marrink, S.; Berendsen, H. A computer Perspective of Membranes: Molecular Dynamics Studies of Lipid Bilayer Systems. *Biochimica et Biophysica Acta* **1997**, *1331*, 235–270.
32. Damodaran, K.; Kenneth, M.; Merz, J.; Gaber, B. Structure and Dynamics of the Dilauroylphosphatidylethanolamine Lipid Bilayer. *Biochemistry* **1992**, *31*, 7656.
33. Damodaran, K. V.; Merz, K. M. A Comparison of DMPC and DLPE Based Lipid Bilayers. *Biophysical Journal* **1994**, *66*, 1076–1087.
34. Smondyrev, A. M.; Berkowitz, M. L. United Atom Force Field for Phospholipid Membranes: Constant Pressure Molecular Dynamics Simulation of Dipalmitoylphosphatidicholine / Water System. *Journal of Computational Chemistry* **1999**, *20*, 531–545.
35. Robinson, A. J.; Richards, W. G.; Thomas, P. J.; Hann, M. M. Head Group and Chain Behavior in Biological Membranes: A Molecular Dynamics Computer Simulation. *Biophys. J.* **1994**, *87*, 2345–2354.

36. Heller, H.; Schafer, M.; Schulten, K. Molecular Dynamics Simulation of a Bilayer of 200 Lipids in the Gel and in the Liquid-Crystal Phases. *J. Phys. Chem.* **1993**, *97*, 8343.
37. Tuckerman, M.; Berne, B.; Martyna, G. Reversible Multiple Time Scale Molecular Dynamics. *J. Chem. Phys.* **1992**, *97*, 1990.
38. Lyubartsev, A. P. Multiscale Modeling of Lipids and Lipid Bilayers. *Eur Biophys J* **2005**, *35*, 53–61.
39. Hyvonen, M. T.; Rantala, T. T.; Ala-Korpela, M. Structure and Dynamic Properties of Di-unsaturated 1 -Palmitoyl-2-Linoleoyl-sn-Glycero-3-Phosphatidylcholine Lipid Bilayer from Molecular Dynamics Simulation. *Biophysical Journal* **1997**, *73*, 2907–2923.
40. Muller, M.; Daoulas, K. C. *NIC Symposium*; John von Neumann Institute for Computing, Ulich, 2008; Vol. 39; Chapter Accurate Measurement of Free Energies of Self-Assembling Systems by Computer Simulation, pp 255–262.
41. Muller, M.; Daoulas, K. C.; Norizoe, Y. Computing Free Energies of Interfaces in Self-Assembling Systems. *Phys. Chem. Chem. Phys.* **2009**, *11*, 2087–2097.
42. Ben-Shaul, A.; Szleifer, I.; Gelbart, W. M. Chain Organization and Thermodynamics in Micelles and Bilayers. I. Theory. *J. Chem. Phys.* **1985**, *83*, 3597–3611.
43. Ben-Shaul, A.; Szleifer, I.; Gelbart, W. M. Chain Statistics in Micelles and Bilayers: Effects of Surface Roughness and Internal Energy. *J. Chem. Phys.* **1986**, *85*, 5345–5359.
44. Al-Anber, Z. A.; Bonet-Avalos, J.; Mackie, A. D. Prediction of the Critical Micelle Concentration in a Lattice Model for Amphiphiles Using a Single-Chain Mean-Field Theory. *J. Chem. Phys.* **2005**, *122*, 104910.
45. Al-Anber, Z. A.; Bonet-Avalos, J.; Floriano, M. A.; Mackie, A. D. Sphere-to-Rod Transitions of Micelles in Model Nonionic Surfactant Solutions. *J. Chem. Phys.* **2003**, *118*, 3816–3826.

46. Pogodin, S.; Baulin, V. A. Coarse-Grained Models of Phospholipid Membranes within the Single Chain Mean Field Theory. *Soft Matter* **2010**, *6*, 2216–2226.
47. Wilson, N. R.; Macpherson, J. V. Carbon Nanotube Tips for Atomic Force Microscopy. *Nature Nanotechnology* **2009**, *4*, 483–491.
48. Vakarelski, I. U.; Brown, S. C.; Higashitani, K.; Moudgil, B. M. Penetration of Living Cell Membranes with Fortified Carbon Nanotube Tips. *Langmuir* **2007**, *23*, 10893–10896.
49. Franz, V.; Loi, S.; Muller, H.; Bamberg, E.; Butt, H.-J. Tip Penetration through Lipid Bilayers in Atomic Force Microscopy. *Colloids and Surfaces B* **2002**, *23*, 191–200.
50. Schrlau, M. G.; Bau, H. H. Carbon-Based Nanoprobes for Cell Biology. *Microfluid Nanofluid* **2009**, *7*, 439–450.
51. Klumpp, C.; Kostarelos, K.; Prato, M.; Bianco, A. Functionalized Carbon Nanotubes as Emerging Nanovectors for the Delivery of Therapeutics. *Biochim. et Biophys. Acta* **2006**, *1758*, 404–412.
52. Almquist, B. D.; Melosh, N. A. Fusion of Biomimetic Stealth Probes into Lipid Bilayer Cores. *Proc. of Nat. Acad. Sci.* **2010**, *107*, 5815–5820.
53. Weast, R. C.; Astle, M. J.; Beyer, W. H. 5th ed.; CRC Press: Boca Raton, Fla., 1984.
54. Wallace, E. J.; Sansom, M. S. P. Blocking of Carbon Nanotube Based Nanoinjectors by Lipids: a Simulation Study. *Nano Letters* **2008**, *8*, 2751–2756.
55. Elbaum, M.; Fygenson, D. K.; Libchaber, A. Buckling Microtubules in Vesicles. *Phys. Rev. Lett.* **1996**, *76*, 4078–4081.

Graphical TOC Entry

